# Reduced high-frequency motor neuron firing, EMG fractionation, and gait variability in awake walking ALS mice

Muhamed Hadzipasic[a], Weiming Ni[b,c], Maria Nagy[b,c], Natalie Steenrod[d,1], Matthew J. McGinley[e], Adi Kaushal[d,2], Eleanor Thomas[a], David A. McCormick[e,f], and Arthur L. Horwich[b,c,f,3]

[a]Interdepartmental Program in Neuroscience, Yale University School of Medicine, New Haven, CT 06510; [b]Howard Hughes Medical Institute, Yale University School of Medicine, New Haven, CT 06510; [c]Department of Genetics, Yale University School of Medicine, New Haven, CT 06510; [d]Sackler Institute Summer Scholar Program, Yale University School of Medicine, New Haven, CT 06510; [e]Department of Neuroscience, Yale University School of Medicine, New Haven, CT 06510; and [f]Kavli Institute of Neuroscience, Yale University School of Medicine, New Haven, CT 06510

Contributed by Arthur L. Horwich, October 10, 2016 (sent for review July 10, 2016; reviewed by George J. Augustine and Monica Gorassini)

**Amyotrophic lateral sclerosis (ALS) is a lethal neurodegenerative disease prominently featuring motor neuron (MN) loss and paralysis. A recent study using whole-cell patch clamp recording of MNs in acute spinal cord slices from symptomatic adult ALS mice showed that the fastest firing MNs are preferentially lost. To measure the in vivo effects of such loss, awake symptomatic-stage ALS mice performing self-initiated walking on a wheel were studied. Both single-unit extracellular recordings within spinal cord MN pools for lower leg flexor and extensor muscles and the electromyograms (EMGs) of the corresponding muscles were recorded. In the ALS mice, we observed absent or truncated high-frequency firing of MNs at the appropriate time in the step cycle and step-to-step variability of the EMG, as well as flexor-extensor coactivation. In turn, kinematic analysis of walking showed step-to-step variability of gait. At the MN level, the higher frequencies absent from recordings from mutant mice corresponded with the upper range of frequencies observed for fast-firing MNs in earlier slice measurements. These results suggest that, in SOD1-linked ALS mice, symptoms are a product of abnormal MN firing due at least in part to loss of neurons that fire at high frequency, associated with altered EMG patterns and hindlimb kinematics during gait.**

ALS | in vivo recording | kinematics | MN firing | EMG

Amyotrophic lateral sclerosis (ALS; Lou Gehrig's disease) is a fatal neurodegenerative disease defined clinically by symptoms of progressive loss of upper and lower motor neurons (MNs). Genetic alterations have been associated with ∼10% of cases, including alterations that affect protein quality or quality control [e.g., mutant SOD1 (superoxide dismutase 1), p97, optineurin, ubiquilin-2] or involve RNA-binding proteins (e.g., TDP43, FUS) (1, 2). Despite the distinct nature of these alterations, they produce similar clinical features, not readily distinguishable from the "sporadic" ALS cases that comprise ∼90% of human cases (3). The network-level alterations and adaptations resulting from chronic MN loss are largely unknown but may be relevant in understanding the disease and designing treatments applicable to all ALS cases. It remains to be seen whether ALS may represent a common process of motor system failure leading to paralysis.

To decipher the progression of motor system failure, mice transgenic for mutant forms of SOD1 have been one of the best models, allowing interrogation of function and biochemistry/morphology at a variety of times within the course to paralysis (4, 5). In this model, there is prominent lower extremity presentation, readily detectable by clinical examination and usually ending in lower extremity paralysis. Thus, studies of SOD1-linked ALS mice have focused on lumbar MNs and the lower extremity (hindlimb) muscles that they innervate. For example, studies of lower extremity muscles in mutant G93A SOD1 mice indicate that denervation is selective to fast-twitch muscle fibers, observed before symptom onset (6, 7). The development of clinical symptoms—lower extremity tremor, twitchiness or clenching, or reduced performance on the rotarod—is associated with MN loss, presumed to involve the MNs that innervate fast-twitch muscle. In a G85R SOD1YFP model of SOD1-linked ALS mice, which become paralyzed by 6 mo of age, we observed that development of such clinical symptoms by 4 mo corresponds to selective loss of low-resistance, fast-firing MNs in acute spinal cord slices prepared from these mice (8). The resulting lack of fast-firing physiology in the context of an in vitro preparation led us to ask: How does the intact G85R SOD1YFP motor system perform motor tasks after selective cell loss in the context of symptomatic degeneration? For a stereotypic, intrinsic behavior such as gait, to what extent are key aspects of the behavior maintained or lost? How is the underlying network output altered? And to what extent does individual MN firing reflect network changes and the loss of fast firing cells? Here we have addressed these questions using recordings from awake mice performing self-initiated walking on a wheel.

## Results

**System for Simultaneous Recording of Extracellular Action Potentials from Single Spinal Cord MNs and EMGs from Lower Leg Muscles of Awake Mouse Walking on a Wheel.** A freely movable light styrofoam wheel system allowed a mouse that was head-post–fixed and spinal-brace–fixed to perform self-initiated walking encouraged by

### Significance

First recordings from awake walking symptomatic-stage amyotrophic lateral sclerosis (ALS) and control mice were made simultaneously from spinal cord motor pools and corresponding hindlimb flexor and extensor muscles. Spinal recordings revealed loss of high-frequency firing in ALS mice, and EMG showed an abnormal fractionated character with step-to-step variability and flexor/extensor coactivation, associated with step-to-step variability in kinematics and likely compensatory mechanisms that allow continued ability to walk in the face of motor neuron loss.

Author contributions: M.H. and D.A.M. designed research; M.H., W.N., M.N., N.S., and E.T. performed research; M.H., M.J.M., and D.A.M. contributed new reagents/analytic tools; M.H., W.N., M.N., N.S., A.K., E.T., and A.L.H. analyzed data; and M.H. and A.L.H. wrote the paper.

Reviewers: G.J.A., Nanyang Technological University; and M.G., University of Alberta.

The authors declare no conflict of interest.

Freely available online through the PNAS open access option.

[1]Present address: Graduate Program in Neuroscience, University of Minnesota, St. Paul, MN 55455.

[2]Present address: University of South Florida, Tampa, FL 33620.

[3]To whom correspondence should be addressed. Email: arthur.horwich@yale.edu.

This article contains supporting information online at www.pnas.org/lookup/suppl/doi:10.1073/pnas.1616832113/-/DCSupplemental.

a reward system, during which simultaneous recordings were taken of EMGs from opposing lower leg muscles and of extracellular spinal cord action potentials from innervating spinal cord MNs (Fig. 1*A*; Figs. S1–S3; *SI Materials and Methods*). The setup includes, as numbered in Fig. 1*A*: (1) a head-post holder mounted on a horizontal crossbar into which can be secured a head post cemented to the mouse's skull, allowing the animal to be fixed atop the wheel (Fig. 1*A*, *Inset*; Fig. S2*A*). (2) Head stages for EMG, mounted so that a plug originating from them can insert into a pedestal cemented to the skull posterior to the head post,

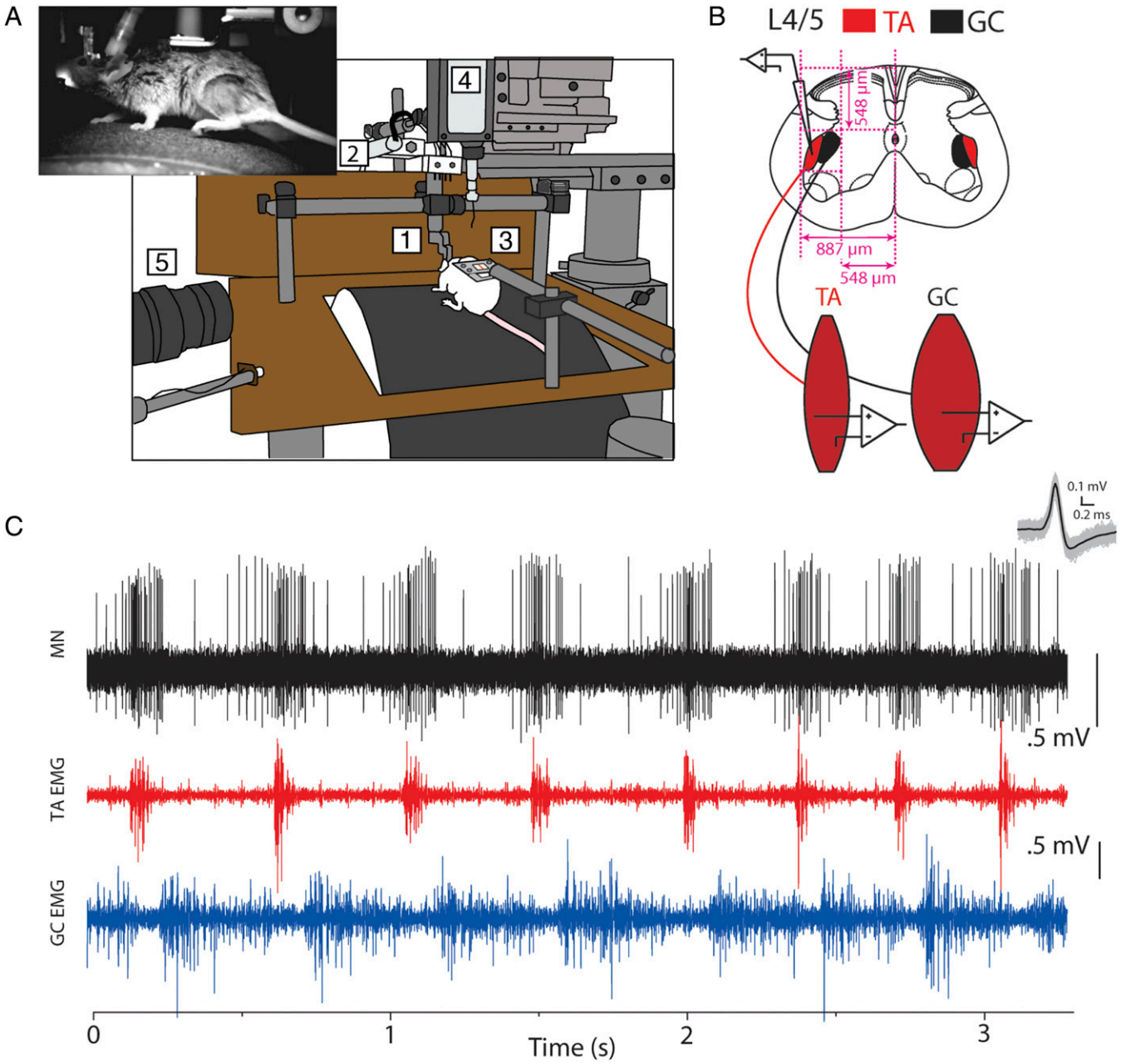


**Fig. 1.** Wheel system for simultaneous in vivo studies of murine gait kinematics, lower leg muscle EMGs, and lumbar spinal cord electrophysiology. (*A*) Diagram of setup with a mouse, head-posted (1) and spine-braced (3) atop a light, movable wheel, allowing the animal to perform self-initiated walking. Head stages for EMG (2) and from spinal cord patch pipette (4) amplify simultaneous recordings of muscle and spinal cord electrophysiology (connections from muscle and cord exposure are detailed in Figs. S2*B* and S3), and a high-speed camera (5) allows for recording of gait kinematics. Animals are acclimated to the environment and encouraged to walk on the wheel through reward-based conditioning (*SI Materials and Methods*). (*Inset*) Lateral view of head-posted and spine-braced mouse walking on the wheel. Note EMG pedestal mounted behind head post. (*B*) Schematic of the recording targets: lumbar spinal cord lateral MN pools (*Top*) and corresponding innervated muscles (*Bottom*). *Top* shows stereotaxic map of L4/5 spinal level with TA (red) and GC (black) MN pools. This guides placement of a 300-µm hole in the coverglass window (see Fig. S3*B* for window placement). By lowering the electrode to a depth of 548–935 µm into the spinal cord at 548–887 µm to the left of the dorsal central artery, the TA and GC pools can be targeted for extracellular single-unit recordings. *Bottom* schematically shows EMG electrodes placed in TA and GC muscles. EMG leads run s.c. up lower extremity and back to a head-mounted pedestal (Fig. S2*B*). (*C*) Example of bursting of an apparent TA MN, recorded as extracellular field potential, the maximum spike rate of which is tightly matched to EMG bursts of TA muscle and anticorrelated to GC muscle during a walking period of a wild-type mouse. (*Inset*) Overlaid spikes and the average spike waveform. Note that the relatively constant voltage of the spikes supports that a single unit is being recorded.

housing EMG leads, led s.c. from electrodes placed in two opposing lower leg muscles, the flexor group including tibialis anterior (TA; flexor of ankle) and the extensor group including gastrocnemius (GC; extensor of ankle) (Fig. S2*B*). (3) A spinal brace modeled after that of Fetcho and coworkers (9), composed of a flat stainless steel plate with a central opening and, at its underside, lateral adjustable bars that clamp the vertebral column, positioned rostrocaudally such that the opening in the plate lies over the L4/5 spinal cord exposed by a one-segment laminectomy (Fig. S3). The brace is fixed via a fork to the platform behind the mouse, allowing the spine to be fixed relative to the wheel (Figs. S1*C* and S3*C*). Within the opening in the plate, a glass window is cemented into place to cover the exposed spinal cord, exerting sufficient pressure to prevent the cord from moving during walking (Fig. S3*B* and *SI Materials and Methods*). (4) Just before the spinal cord recording, a hole is drilled into a lateral position of the glass window directly over the lateral TA/GC motor pools at L4/5 (Fig. 1*B*), through which a pulled glass pipette (10-μm tip diameter, 4–7 MΩ resistance) attached to a microelectrode headstage (4) is slowly lowered, while recording, through the dorsal cord to the appropriate depth of the TA/GC motor pool via a micromanipulator. (5) A high-speed camera (Fig. S1*C*) captures walking motion on the wheel from one side (Fig. 1*A*, *Inset*); infrared-reflective microdots glued to relevant joints of the lower extremity enable video recording of kinematics.

An example of a simultaneous recording from a 4.5-mo-old transgenic wild-type SOD1YFP control mouse walking on the wheel is shown in Fig. 1*C*. The recorded bursts of neuronal firing are temporally correlated to EMG bursts from the flexor (TA) muscle and are anticorrelated to bursts from extensor (GC) muscle, identifying the spinal cord electrode as lying within the "TA" motor pool. The burst likely derives from a single MN because the spikes all exhibit similar voltage and waveform. Thus, MN firing and simultaneous muscle output can be examined in wild-type SOD1YFP mice (that do not develop motor disease) and compared with recordings from symptomatic G85R SOD1YFP ALS mice.

**ALS Mice at 4.5 Mo Exhibit Reduced Gastrocnemius M-Wave Amplitude but Maintain Lower Extremity Stride Length.** In a previous study, we observed that transgenic G85R SOD1YFP mice first exhibit clinical symptoms at 3–4 mo of age, usually manifested as clenching of the lower extremities when picked up by the tail, and reduced performance in the rotarod test (8). This was associated with a loss of ∼50% of large choline acetyltransferase (ChAT)-positive spinal cord MN cell bodies from the ventral horns compared with age-matched wtSOD1YFP control mice. A further loss of ∼50% of the remaining MN cell bodies occurs by the time of lower extremity paralysis, occurring typically at 6 mo of age. In seeking to determine a time point at which to study single MN functional output, we interpolated between these times, examining 4.5-mo-old mice. Motor unit loss was first quantified in vivo by changes in whole-muscle compound action potential (M wave) amplitude. M waves from the gastrocnemius muscle of anesthetized mice were evoked by bipolar stimulation of the sciatic nerve (Fig. 2*A*, *Top*) and measured as peak-to-peak amplitude (Fig. 2*A*, *Inset*; *SI Materials and Methods*). In 4.5-mo-old G85R SOD1YFP mice, M-wave amplitude is reduced fourfold relative to age-matched wtSOD1YFP mice (6.5 ± 1.2 mV vs. 25.9 ± 2.4 mV, $P = 3.6 \times 10^{-4}$). This reflects extensive reduction of functional motor units and is morphologically correlated with loss of MNs in the lateral TA/GC motor pool (8), loss of axons in lumbar ventral nerve roots (Fig. 2*B*, *Left*), reduced gastrocnemius muscle fiber area (Fig. 2*B*, *Right*), and loss of gastrocnemius fast-fatiguable (anti-myosin IIb antibody-reactive) muscle.

Despite reduced M waves associated with extensive MN loss and reduction of functional motor units, gross motor output of the ALS mice, measured as lower extremity stride length of head-fixed animals on the wheel, was maintained at 4.5 mo and beyond (>140 d),

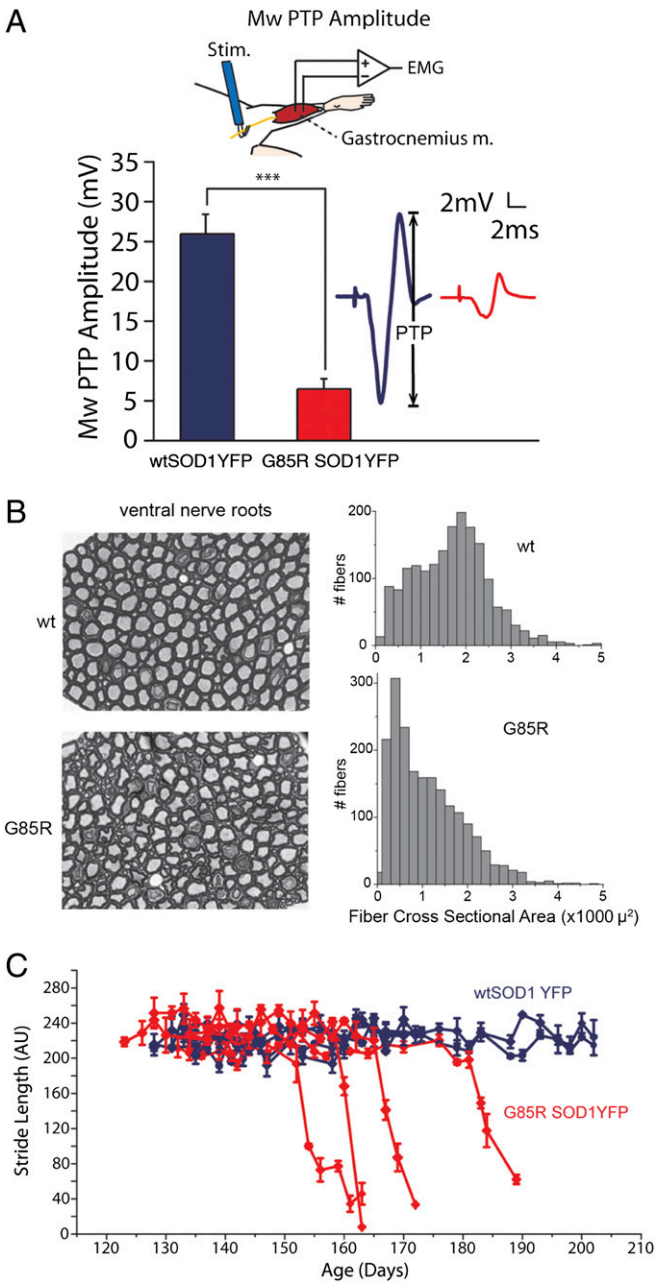


**Fig. 2.** Reduction of whole gastrocnemius action potential (M wave), abnormal ventral nerve root motor axons, and reduced gastrocnemius muscle fiber diameter, but maintained stride length, in 4.5-mo-old G85R SOD1YFP mice. (*A*) Whole-muscle compound action potentials (M wave) from the gastrocnemius muscle evoked by bipolar stimulation of the sciatic nerve in 4-mo-old G85R SOD1YFP mice and age-matched wtSOD1YFP controls. Setup is shown in *Top* image. M waves were measured via peak-to-peak (PTP) amplitude on whole-muscle EMG (*Right*). In mutant, M-wave amplitude measures 6.5 ± 1.3 mV, and in wild type, 25.9 ± 2.5 mV, corresponding to a fourfold reduction in the mutant mice ($P = 3.6 \times 10^{-4}$). This reflects substantial loss of functional motor units. (*B*) Abnormality of ventral nerve root (motor) axons (*Lower Left*) in mutant at 4.5 mo, including fragmentation, jagged shapes, and notable gaps, likely reflecting lost axons, relative to the regular "cobblestone" appearance of age-matched wtSOD1YFP mice. When cross-sections of lateral gastrocnemius muscle fibers, outlined by staining with anti-dystrophin antibody, were measured for fiber area at the same level of the muscle in mutant and wild type (*Right* panels), the distribution of fiber areas across the mutant muscle was reduced. (*C*) Despite motor unit loss, gross motor output as measured by stride length of head-fixed animals on the wheel is maintained at 4.5 mo and is reduced only a few days before paralysis at 5–6 mo of age (red traces); wild type shown in blue (see text).

only becoming reduced several days before lower extremity paralysis (Fig. 2*C*: compare red, mutant, with blue, WT; see figure 1F in ref. 4). The preservation of stride length late into the disease course motivated a kinematic analysis of G85R SOD1YFP gait to determine whether specific alterations emerged in the context of compensated overall output.

**Gait Kinematics of 4.5-Mo-Old Wild-Type and ALS Mutant Mice: Step-to-Step Variability and Forward Position of Hindlimb.** Control and mutant animals were head-fixed to the wheel and acclimatized until they comfortably performed self-initiated walking. IR reflective dots were then fixed to the iliac crest, hip, knee, ankle, and metatarsophalangeal (MP) joint, and animals were videotaped while walking so that hip, knee, and ankle angles could be tracked continuously throughout gait (see *Materials and Methods* for details). Consistent with a maintained stride length, hip, knee, and ankle angle, minimum, maximum, range, mean, and takeoff were maintained (Fig. S4 *A*–*C*). However, when examining individual traces that are the average of hip, knee, and ankle angle across many steps for each animal, the variability of the average traces across mutant animals was notably increased relative to wild type (Fig. 3 *A*–*F*; navy blue curve for each wild-type animal; red curves for each mutant mouse; see Fig. S5*A* for quantitative analysis). Intra-animal step-to-step analysis also showed significantly greater variance in the mutant for knee and ankle angles (Fig. S5*B*).

The mutant variability made it difficult to establish quantitative differences in specific measures of gait. Qualitatively, however, a feature unique to most mutant mice was a consistently more forward positioning of the hindlimb through the gait cycle (see Fig. 3 *G* and *H* for example). This was evident both at the start and the completion of the stance phase, during which the paw moves upon a surface to propel the mouse forward (Fig. 3 *G* and *H*, first three panels). In the average gait cycle, this manifests as a more forward positioned leg throughout the step cycle (horizontal position of ankle at the beginning of swing phase, Ankx, Fig. 4, 384 ± 43 wild type vs. 361 ± 47 in mutant, $P = 0.0017$). Consistent with this, most of the ALS mice at 4–5 mo of age exhibit a thoracic kyphosis, a function of either defective MN innervation of the thoracic region or altered descending postural control.

Hence, although G85R SOD1YFP mice are able to generate normal stride length, motor output during gait is less stereotyped and more variable from step-to-step both for an individual mouse and in the mutant mice as a group. These changes in overall output led us to seek associated changes in network output as measured by EMG.

**ALS Mutant Mice Display Fractionated ("Reduced Interference Pattern of") Leg Muscle TA and GC EMGs and Increased Cocontraction.** EMGs from TA and GC were first measured while head-fixed 4.5-mo-old mice walked on the wheel. The swing phase of gait commences when the horizontal position of the ankle is fully posterior (see Fig. 3 *G* and *H*, third panels; Fig. 4 *A* and *B*, Ankx). The onset of swing is associated with TA muscle activity and commencement of dorsiflexion of the ankle. In wtSOD1YFP mice (Fig. 4*A*, *Top* trace and blue in overlay of phases in *Right* panel), TA EMG comprises a brief phase of activity (~50 ms), shortly followed by an envelope of GC activity (~250 ms; gray in *Right* panel) associated with stance phase. In striking contrast, the recording strips of a 4.5-mo-old G85R SOD1YFP mouse (Fig. 4*B*) show different patterns of both TA and GC activity.

TA activation appears to commence at the normal time, relative to maximum Ankx. However, lower-amplitude irregular bursts of TA activity often followed the large initial burst, carrying TA activity into stance phase (Fig. 4*B*, overlaid EMG traces from the fourth cycle; Fig. 4*B*, *Right*; TA, red; GC, gray). In an average from 202 steps (six mice), this "fractionated output" appears as a second smaller TA peak not present in wild type (156 steps, five mice; Fig. S6, *Top*, red trace). Mutant GC EMG activity appears to initiate slightly earlier than in wild type following the initial TA burst (average in Fig. S6, *Bottom*, red trace; 202 steps, six mutant mice) and is again marked by irregular fractionated output that varies from cycle to cycle, compared with the regular envelope of activity in wild type (average in Fig. S6, *Bottom*, black trace; 156 steps, five mice; see also GC traces in Fig. 4). The fractionation of GC EMG could reflect a reduced number of active MNs.

To quantify the fractionated mutant EMG patterns, we first calculated the average power spectra of TA and GC EMG for mutant and wild-type mice (Fig. S7*A*, *Left*, TA; Fig. S7*C*, *Left*, GC; wild type, blue, $n = 5$; mutant, red, $n = 6$). In mutants, these spectra seemed to be right-shifted, biasing toward higher frequencies. Indeed, in the group average power spectra (Fig. S7 *A* and *C*, *Middle*), mutant spectra displayed additional high-frequency peaks (red arrows). This could be consistent with the greater number of single-motor-unit potentials (Fig. S7 *B* and *D*, *Right*, arrowed in mutant). Cumulative density functions (CDFs) of the normalized power spectra showed that, in both TA and GC muscles, mutant EMGs contained more high-frequency content (Fig. S7*A*, *Right*, TA; Fig. S7*C*, *Right*, GC; mutant, red traces, green average; WT, blue traces, cyan average; Kolmogorov–Smirnov (K–S) tests, $P = 0.018$ and $P < 10^{-5}$, respectively). For TA, mutants displayed significantly higher 75th percentile CDFs (approximately half-way between starting density and 1.0; 36.4 ± 8.5 Hz vs. 21.2 ± 10.5 Hz, $P = 0.026$; Fig. S7*B*, *Left*), and for GC, CDFs trended toward a higher 90th percentile (approximately halfway between starting density and 1.0; 40.9 ± 24.1 Hz vs. 12.1 ± 4.8, $P = 0.07$; Fig. S7*D*, *Left*).

We also carried out a quantitative analysis of overlap in TA and GC activity (cocontraction). We rectified and smoothed corresponding TA and GC EMG traces, normalized to step-cycle length, and for each mouse calculated the average percentage of the step cycle during which TA and GC simultaneously exceeded 10% of their respective step cycle maximum values (see Fig. S8*A* comparing WT, *Top*, and mutant, *Bottom*, for example). Mutant animals displayed significantly higher cocontraction (Fig. S8*B*, 29.5 ± 16.3% vs. 12.7 ± 7.8%, $P = 0.0047$). Interestingly, such an increase of cocontraction has been reported in human spinal cord injury in the setting of muscle weakness, likely serving to activate muscles continuously as a means to propel forward and remain upright (10).

Thus, in 4.5-mo-old ALS mice, variable gait output is generated by fractionated hind-limb EMGs that lack precise onset and offset timing, leading to increased cocontraction. To investigate how firing patterns of individual units could contribute to fractionated output, we recorded single spinal motor units and hindlimb EMG simultaneously in walking mice.

**Single-Unit Recordings in 4.5-Mo-Old ALS Mice Lack Precisely Timed, High-Frequency Output.** Given the well-defined role of MNs in transducing the network output mediating normal gait, we measured the firing profiles of single MNs in the context of the abnormal EMGs just described. Single-unit extracellular recordings were taken from a pulled glass microelectrode lowered into the adjoining TA and GC motor pools using stereotaxic guidance, allowing comparison of firing of individual motor units from these pools in walking head-fixed and back-braced wild-type and ALS mutant animals at 4.5 mo of age (Figs. 5 and 6). Given the technical barriers to making measurements of this nature, we were not able to confirm the identity of putative TA or GC MNs other than by noting their stereotaxic position and the tight temporal correlation of their firing with TA or GC EMG signals. In a more formal analysis, spike-triggered averaging (Fig. S9) showed in many cases a temporal relationship between a spike of, for example, putative TA MN firing and TA EMG response. Thus, in the discussion below, reference to single units as TA or GC MNs reflects identification by the aforementioned criteria. In wild type, the changes in instantaneous firing frequency of individual units closely matched the rectified, smoothed EMG. In the ALS mutant, the low instantaneous firing

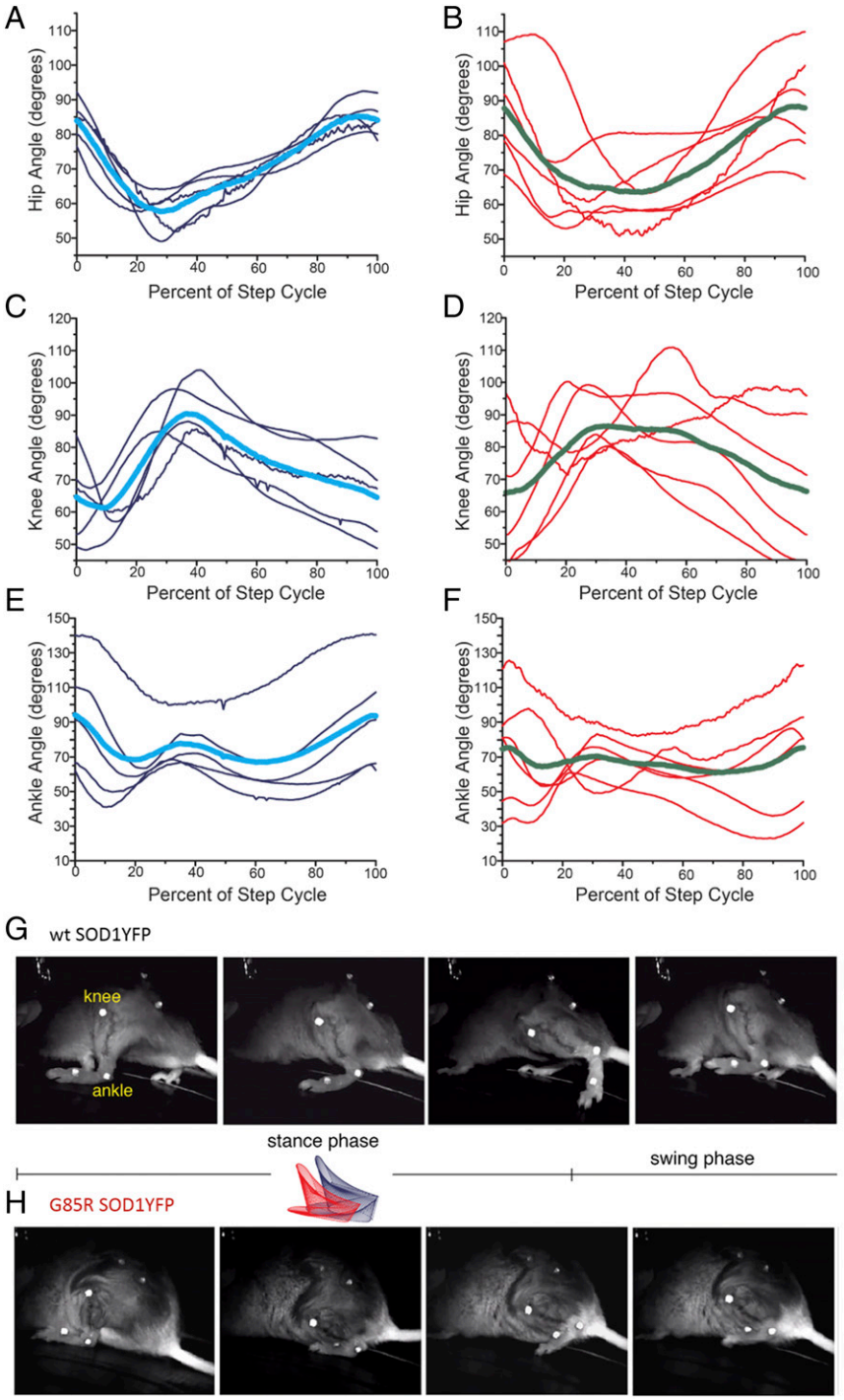


**Fig. 3.** Altered gait kinematics. (*A–F*) Traces representing averages of hip, knee, and ankle angles in wtSOD1YFP mice (*A*, *C*, and *E*, respectively) and G85R SOD1YFP mice (*B*, *D*, and *F*, respectively) during the step cycle. The *y* axis (0%) denotes transition from stance to swing; note that conversion from swing to stance phase occurs at ∼30% of the cycle. The average trace of four individual mice is shown in the *Left* panels in navy blue with the average in cyan, and the average trace of six mutant mice is shown in the *Right* panels with the average in green. Variance measurements, both interanimal and intra-animal, are given in Fig. S7, showing the significant increase of variance of gait between mutant mice in Fig. S7*A* and between steps of mutant mice compared with wild type in Fig. S7*B*. (*G* and *H*) Frames from video recordings of walking on the wheel showing (left to right) the start, middle, and end of stance phase and the middle of swing phase of gait, for wtSOD1YFP (*G*) and G85R SOD1YFP (*H*). Red/blue *Inset* shows superposition of average of lower leg position of wild type (blue) and mutant (red) through stance phase at 2% intervals. The mutant mouse stands in a hunched posture on the wheel (not shown), which may account for the average position of its hindlimb being more anterior than wild type at the start of stance. For the same stride length, the mutant animal thus completes stance with the limb more anterior.

frequency and irregularity of MN burst patterns coincided with the fractionated EMGs.

***Tibialis anterior.*** In a representative single-unit recording of a wild-type TA MN in a 4.5-mo-old wild-type animal walking on the wheel (Fig. 5*A*), regular bursts of firing were observed, with the highest frequency within a burst corresponding to the peak of the rectified smoothed EMG (see *Bottom* trace reporting instantaneous MN firing frequency). Typically, spiking begins at a low frequency followed by a sharp increase in instantaneous firing (carried by approximately five spikes) that coincides with the peak of EMG. This corresponds well to the behavior of MN firing and simultaneous EMG previously reported in a cat walking on a treadmill (11). In contrast with wild type, an ALS TA motor unit in a 4.5-mo-old animal (Fig. 5*B*) exhibits bursts with a visibly lower frequency of firing and only a modest correlation of increased firing rate with peaks of EMG (compare green and red traces in Fig. 5*B*; note that the rectified and smoothed EMG trace does not clearly show the extended low-amplitude muscle activity observed in the raw trace of Fig. 4*B*).

The intraburst structure of firing of the two TA MNs (of Fig. 5 *A* and *B*) was further examined by aligning a collective of their bursts on raster plots (top to bottom, each spike as a dot; Fig. 5 *C* and *D*), 134 bursts of the wild-type cell (four bursts of which are shown in Fig. 5*A*) and 82 bursts of the mutant cell (four bursts of

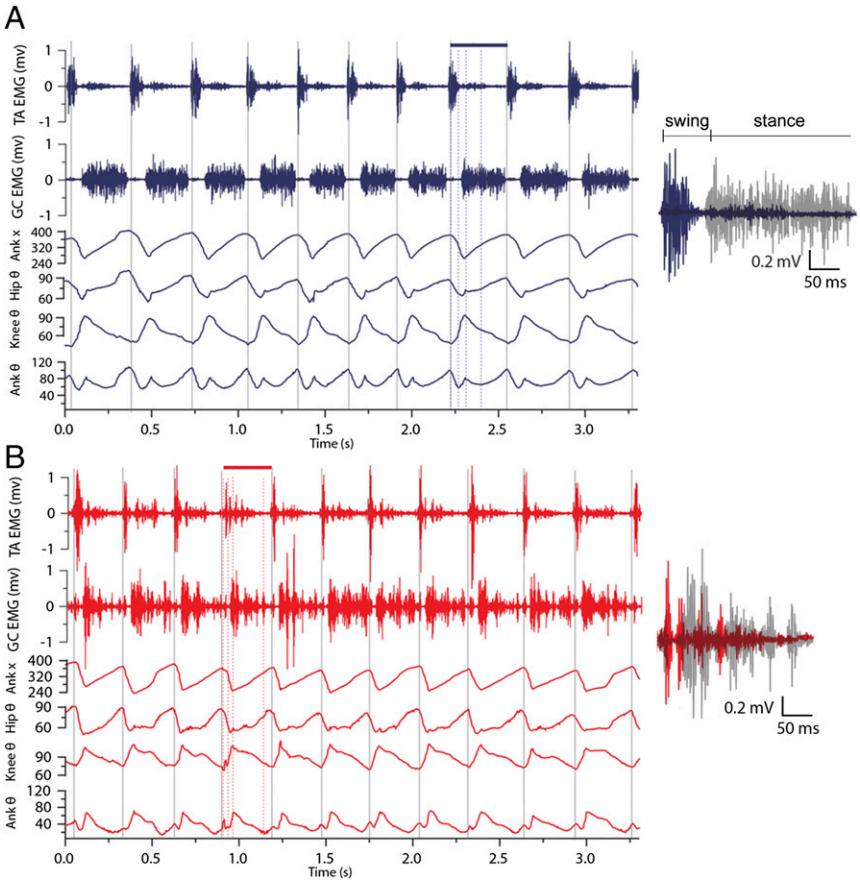


**Fig. 4.** TA and GC EMGs (*Top* traces) of a representative wild-type mouse (*A*) and ALS mutant mouse (*B*) and corresponding kinematic measurements (*Bottom* traces) of ankle position on the horizontal axis (Ankx, measured as pixels from video recording), as well as hip, knee, and ankle angles (Θ) during a walking period. In *A*, dashed blue vertical lines between 2.2 s and 2.6 s for wild type show start of swing, midswing, start of stance, and midstance. Image at *Right* shows overlaid wild-type TA (blue) and GC (gray) EMG traces for segment under the blue bar (see text). Maxima of ankle horizontal axis position were used to segment traces into steps (commencing at start of swing) as indicated by the solid gray vertical bars. (*B*) Same as in *A* but in red, representative of G85R SOD1YFP mutant. Note that both TA and GC EMG traces appear "choppy" (fractionated) relative to wild type and are variable from burst to burst, with overlap of signals (cocontraction) as shown in the *Right* overlay panel of TA (red) and GC (gray) for the segment under the red bar.

which are shown in Fig. 5*B*). Motor unit activity was temporally matched with the EMG with 100 ms of recorded spiking on either side of the peak of EMG potential (the latter shown below the raster plots). Examining the raster plot for the wild-type MN, a well-defined burst in motor unit firing emerges where a rapid increase in the frequency of spikes [shown in the summary graph below the raster; cyan trace, periburst spike histogram (PBSH)] occurs synchronously with the peak of the EMG (dark blue trace; note that the individual traces of all EMG recordings, rectified and smoothed, are shown in gray). The bursts from two representative raster traces are shown to the right (asterisked in the raster plot at left in Fig. 5*C*), where the EMG peak (dark blue trace; centered at 0 ms) corresponds closely with the increase of instantaneous spike frequency (cyan trace).

In contrast with the wild-type pattern, the mutant raster plot matching MN firing (PBSH, green, in summary plot below raster) with the peak of EMG (red peak) shows no distinctive burst in motor unit firing (Fig. 5*D*). This is illustrated by plotting the instantaneous firing rates from two example raster lines (asterisks in the plot at left). In these traces, the EMG pattern is sufficiently choppy that a single EMG peak cannot be clearly identified. Selecting the highest amplitude of EMG as peak and examining the matching window of motor unit firing, there is no clear peak of MN firing but just a small increase of firing over the swing phase. In the summary plot of the raster for the mutant (Fig. 5*D*, *Bottom*), relatively uniform spiking (green trace) is observed across the 200-ms window. Thus, for TA MN firing, in wild type there is a prominent increase of MN firing frequency associated with the EMG peak. In the mutant, however, there is at best only a small and temporally diffuse increase of firing frequency, and the output EMG appears correspondingly choppy. Nevertheless, considering all cycles, the averaged EMG shows an overall peak (red; see collective of all smoothed EMG traces in gray).

***Gastrocnemius.*** In wild type, the sustained EMG burst pattern of GC activity was associated with steady and maintained firing of single motor units recorded during stance phase (Fig. 6*A*, MN and Inst.MN Firing Freq.). In the ALS mutant, by contrast, there is a burst of action potentials at the onset of a GC EMG burst that quickly dissipates throughout the latter period of the stance phase during the fractionated EMG (Fig. 6*B*). For GC, the raster plot of MN spiking was aligned to the start of the EMG burst at the beginning of the stance. In wild type (74 bursts in raster plot), motor unit firing jumps to a high rate at the start of EMG and remains high throughout the EMG burst (Fig. 6*C*; see summary plot below raster for 179 steps, blue for EMG and cyan for PBSH). This is observed also in the two representative traces for wild type. In the mutant, in contrast, there is only an early burst of spiking, followed, in some cases, by a train of spiking but in many others by either sparse firing or no further firing (Fig. 6*D*; see raster plot, 78 bursts). The summary plot below the raster (209 steps mutant GC) reflects the initial rise in spike frequency followed by a rapid fall after ~100 ms (green trace). EMG (red trace) is maintained, however, to what corresponds to the end of the few observably fully intact spike trains.

**Reduced Instantaneous Firing Frequency of ALS MNs.** The TA MN firing behavior was examined for six wild-type and five ALS neurons in relation to EMG peak (Fig. 7*A*). First, the mean instantaneous firing frequency was plotted for wild type and mutant at three times: 100 ms before the EMG peak, at the peak, and 100 ms following the peak (colored points). Although the mean firing frequencies at the preceding and following time points were not significantly different, at the peak of EMG, the wild-type instantaneous

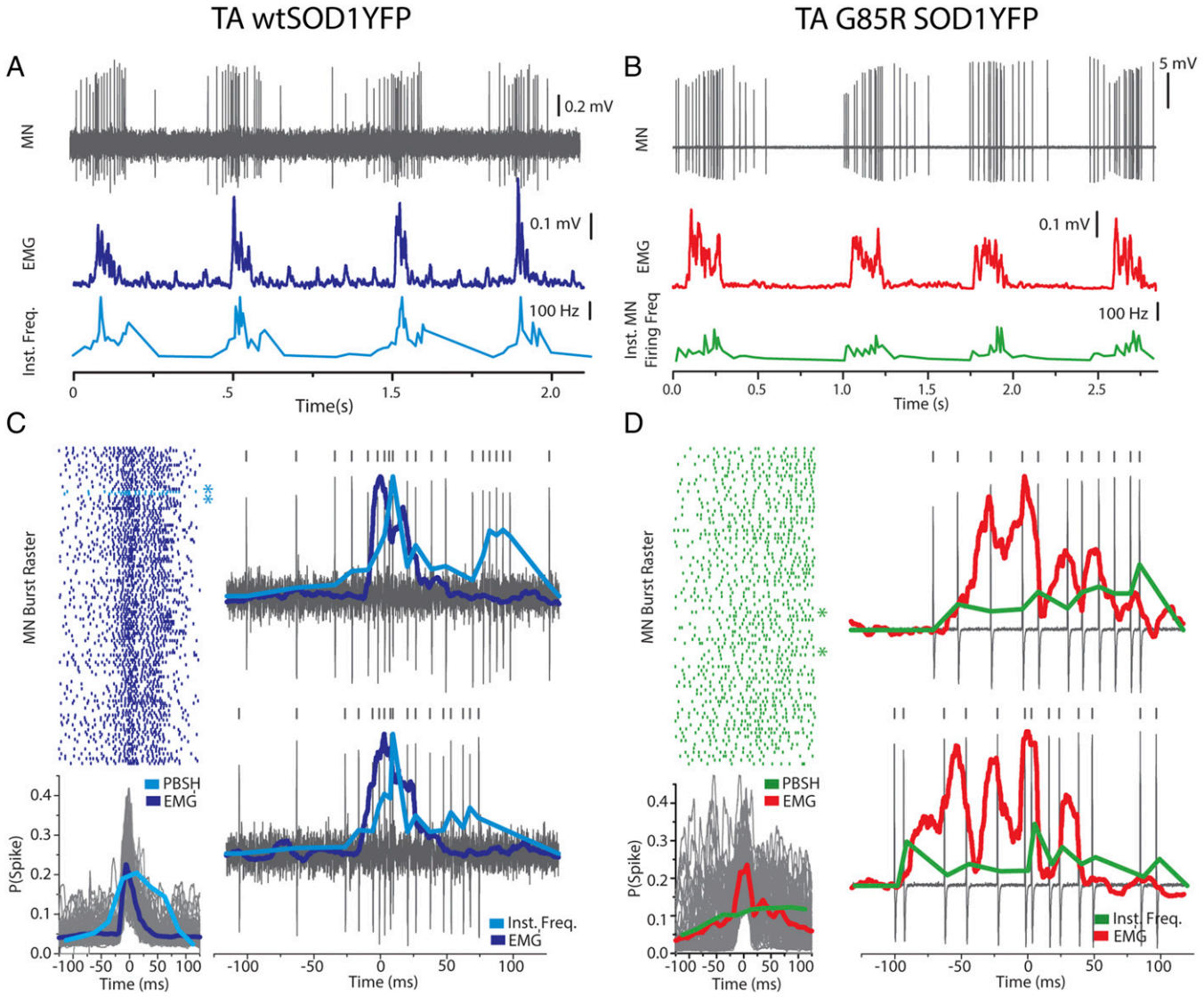


**Fig. 5.** High-frequency action potential output of wild-type TA MNs during walking is EMG-correlated, whereas lack of high-frequency output from mutant TA MNs produces variability of TA muscle EMG. (*A*) Representative single-unit extracellular recording of a TA MN in a 4.5-mo-old control animal along with corresponding rectified smoothed TA EMG and instantaneous MN firing frequency. The instantaneous firing frequency visibly correlates with TA EMG, and frequencies greater than 300 Hz are regularly obtained. (*B*) Representative single-unit recording of a TA MN in a 4.5-mo-old G85R SOD1YFP mouse shows the same choppy EMG signal as in Fig. 4*B* (here rectified and smoothed). Instantaneous firing frequency of the mutant MN also visibly corresponds to the choppy EMG, but the frequencies obtained are markedly lower than in control, and there is no single prominent peak of firing (green trace). (*C*, *Left Upper*) A raster plot of 134 bursts during walking from the cell in *A*, aligned to the peak of the rectified and smoothed TA EMG. (*Left Lower*) The overlaid EMG bursts (gray) with their average (blue), as well as the periburst spike histogram (PBSH, cyan), calculated from the raster. Note that a 200-ms "window" of MN bursting is shown, centered at zero on the peak of EMG. The raster and summary plot show a sharp increase in the probability of spiking precisely timed to EMG onset. (*Right*) Two sample bursts from the raster (indicated by cyan asterisks). Within each burst there is a slow increase in spike rate before changes in EMG and then sharp rapid increases in spike rate corresponding to EMG onset. In some TA bursts (e.g., *Upper* example) there is a second rapid discharge, whereas in others there is not (*Lower* example). (*D*) As in *C*, for 82 bursts during walking from the mutant cell in *B* in red and green. Note that there is a lack of precisely timed high-frequency MN output for the mutant cell, which manifests as a sparse raster and flat PBSH. The average mutant EMG (red, *Lower*) shows the same choppiness and second peak as in Fig. 4*B*. (*Right*) Two expanded mutant bursts (green asterisks in raster) show a lack of the sharp increases in MN spike rate that occur following the slow increase of spiking seen in the wild-type mouse (*C*).

firing frequency was significantly greater than mutant, measuring 142.8 ± 3.9 Hz vs. 69.7 ± 3.2 Hz ($P = 0.0027$).

Instantaneous firing frequencies were also plotted for the entire burst periods of all of the in vivo-recorded TA and GC MNs of wild type and ALS mutant and plotted as histograms (Fig. 7*B*). Here, there is a notable leftward skew of the mutant histogram, reflecting a greater fraction of firing at lower frequencies. This is quantitated in Fig. 7*C* (In Vivo) where the percentiles of firing frequency in relation to the histograms are enumerated. In particular, the median firing frequency for wild type is 122 Hz, whereas for the mutant it is 71 Hz. Similar differences are seen for the various percentiles, and the mode (the most repeated frequency) is 85 Hz for wild type and 45 Hz for mutant. Notably also, the "tail" of the wild-type histogram contains a much more substantial fraction of firing at frequencies >200 Hz (25% vs. 7% for ALS mutant). This is of particular importance because these high frequencies correspond in wild type to the burst of spiking observed at the peak of EMG (see, e.g., Fig. 5*A*, Inst. Freq.).

The reduced instantaneous firing frequency in vivo by the ALS mutant MNs corresponds, strikingly, with observations obtained

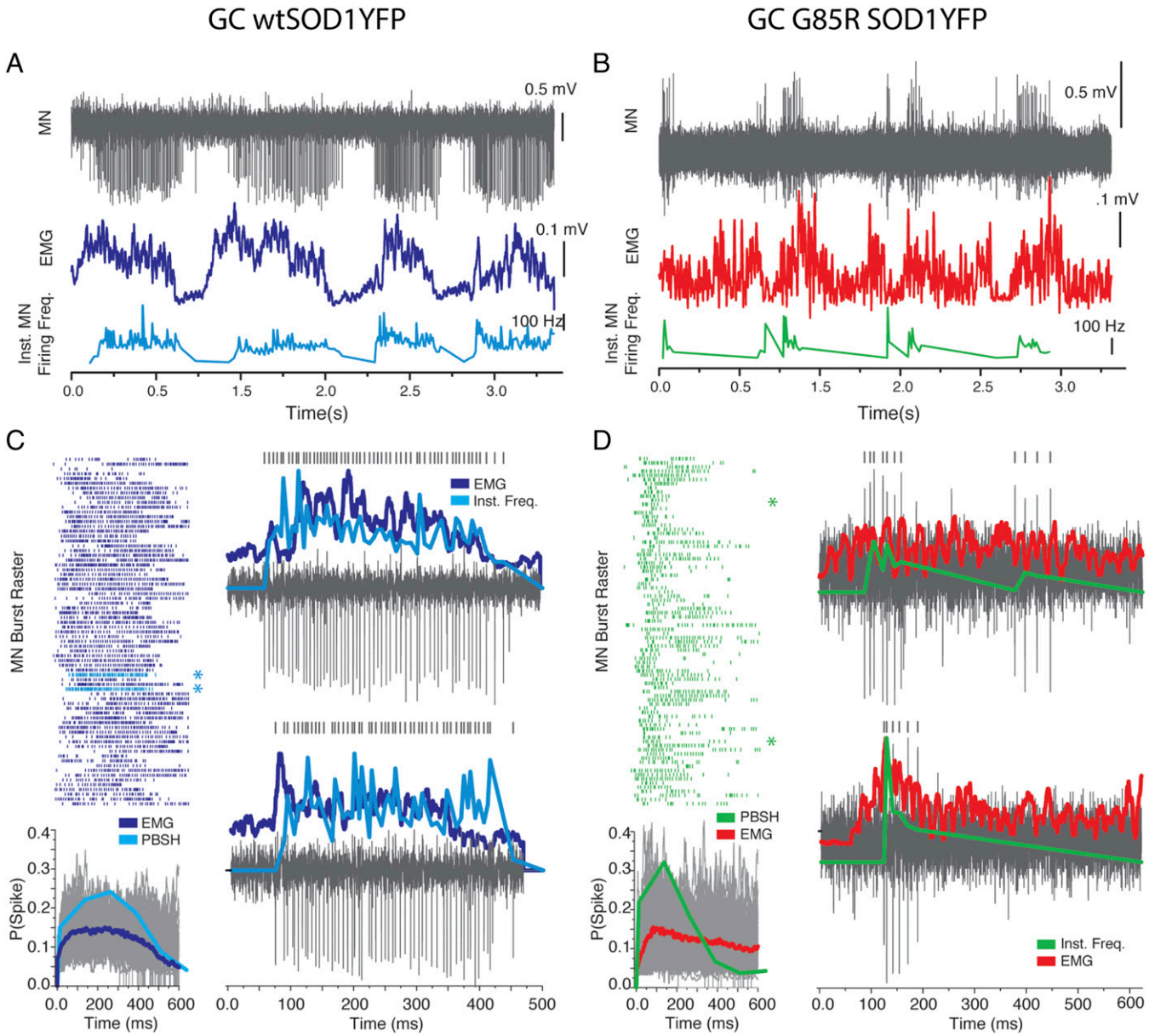


**Fig. 6.** Sustained high-frequency action potential burst of GC MNs during walking produces steady EMG firing in wild type whereas in the mutant premature dropoff of high-frequency output from mutant GC MNs produces choppy EMG that varies from burst to burst. (*A*) Representative single-unit extracellular recording of a GC MN in a 4.5-mo-old control animal, along with corresponding rectified smoothed GC EMG and instantaneous MN firing frequency. The instantaneous firing frequency visibly correlates with GC EMG, and frequencies greater than 200 Hz are regularly obtained. (*B*) Representative single-unit recording of a GC MN in a 4.5-mo-old G85R SOD1YFP mouse showing regular bursts but of much shorter duration than in wild type. The same choppy EMG signal is observed as in Fig. 4*B* (here rectified and smoothed). The instantaneous MN firing frequency shows an initial high-frequency burst that then dissipates. (*C*, *Upper Left*) A raster plot of 74 MN bursts during walking from the cell in *A*, aligned to the start of EMG firing. (*Lower Left*) The overlaid EMG bursts (gray) with their average (blue), as well as the periburst spike histogram (PBSH, cyan), calculated from 179 steps. Note that the "window" length here is 600 ms in duration, encompassing most wild-type bursts. The raster and summary plot show a broad increase of probability of spiking precisely timed to the envelope of EMG. (*Right*) Two sample bursts from the raster (indicated by cyan asterisks). Within each burst there is a definable increase in spike rate that corresponds to EMG onset and that is then sustained across the EMG envelope. Overall, one wild-type GC was examined, with 179 steps total. (*D*) As in *C*, but red/green with raster composed of 78 bursts during walking from the mutant cell in *B*. Note for the mutant cell that there is a regular occurrence of what appears to be a bifid high-frequency MN firing that then dissipates prematurely. The second peak of MN firing is associated with EMG bursting (rectified and smoothed), which then lessens and is choppy in character. The raster and summary plot (for 209 steps total from two mutant GC MNs) show that there is the rapid rise of probability of firing to 100 ms, but that probability of firing then falls markedly, corresponding to the representative behavior of *B*. Some lines of the raster show continued firing across 600 ms, and, interestingly, average EMG (red) is sustained across the period. Thus, despite frequent dissipated MN bursting (raster and two representative bursts to right), overall EMG firing seems retained and is sufficient to drive stance phase of gait (Fig. 3).

earlier for MN firing in acute spinal cord slices prepared from wild-type and ALS mutant animals of 4 mo of age (8). In that study, patch clamp-recorded MNs from wild-type animals and 2-mo-old mutant animals could be grouped into four clusters, related to first instantaneous firing frequency and steady-state firing frequency (upon current injection of 3× rheobase). Both wild-type MNs and those studied from ALS mutant mice at 2 mo of age exhibited comparable numbers from the four clusters. By

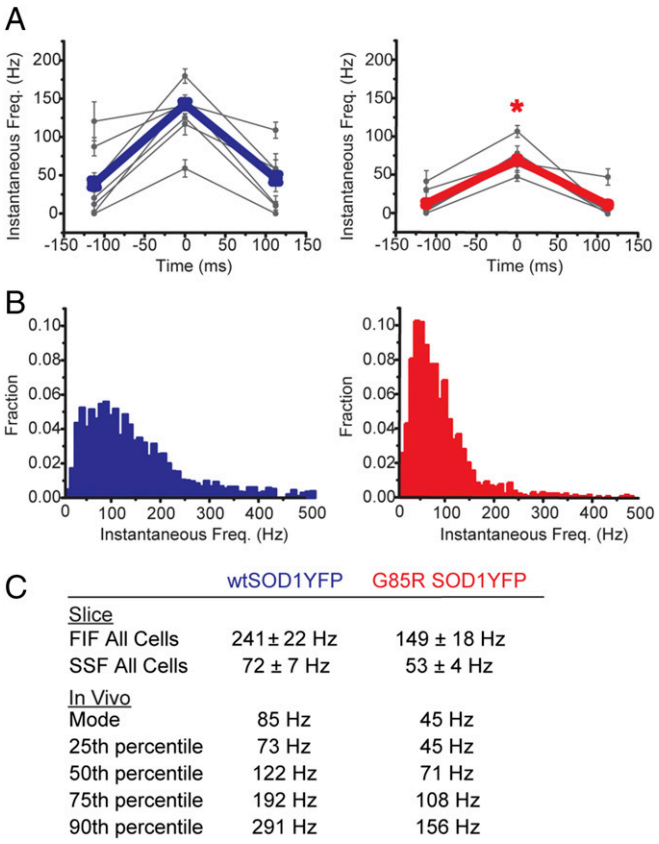


**Fig. 7.** Reduced instantaneous firing frequency of ALS MNs in vivo and in slice from 4-mo-old G85R SOD1YFP mice. (*A*) Population data from TA MNs recorded in vivo at 4.5 mo of age during walking on the wheel, six wild-type SOD1YFP neurons (*Left*, blue) and five G85R SOD1YFP neurons (*Right*, red). Dark blue or red points indicate respective wild-type or ALS mutant mean instantaneous firing frequency at three times: 100 ms before EMG peak, at peak EMG, and 100 ms after EMG peak. The means and SEs for the individual MNs of each type are shown as small points connected by thin lines. Red asterisk indicates that the mutant value is different from that of wild type with a $P$ value = 0.0027. (*B*) Normalized histograms showing instantaneous firing frequencies attained by the population of wild-type (blue) and mutant (red) TA MNs during bursts. Note the leftward skew of the histogram of mutant toward lower frequencies, and note that the "tail" portion firing at greater than 200 Hz is far more populated for wild type than for the mutant (see text). This has implications for attaining proper MN bursting at the peak of EMG (see Fig. 5 legend and *Discussion*). (*C*) Comparison of firing frequencies (first instantaneous and steady state) of ventral horn MNs obtained earlier by patch clamp recording from acute slices from the same mouse strains at 4 mo of age (8) with those from in vivo recordings, here at 4.5 mo, from combined TA and GC during walking. In both settings, the collective of mutant MNs fire at lower frequency than the collective of wild type (see text).

4 mo of age, however, whereas the distribution in wild type was unchanged, the ALS mutant exhibited none of the fastest-firing MNs and a reduced number of the next-fastest firing MNs. Summing up the firing data from all of the MNs studied at 4 mo in each of wild-type and ALS mutant slices produces, respectively, first initial firing rate and steady-state firing rates as shown in Fig. 7*C*, lines 1 and 2, that exhibit a reduction in slice in the ALS mutant similar to that observed here in vivo (lines 3–7).

Hence, in 4.5-mo-old ALS mice, individual MNs fire at frequencies consistent with preferential loss of the fastest-firing MNs, as observed in slice studies. As a result, frequencies seen in the mutant are significantly slower, and cells fail to generate the same sharp, precisely timed increases in spike rate seen in wild-type mice.

## Discussion

**Loss of High-Frequency MN Firing, Fractionated EMG, and Variable Gait Output in ALS Mice.** The simultaneous in vivo recordings presented here from spinal cord MNs and their innervated muscles in awake, walking mice provide a view of both normal MN output in wild-type mice and impaired output in mutant SOD1 transgenic ALS mice at a stage when the mice are symptomatic (4.5 mo), but before paralysis (6 mo). A principal finding is that, in the mutant (G85R) SOD1YFP-transgenic ALS mice, MNs exhibit reduced instantaneous firing frequency at 4.5 mo, measured as extracellular single-unit recordings, compared with age-matched control mice transgenic for wild-type SOD1YFP. The simplest explanation for reduced instantaneous firing frequency is loss of the fastest-firing MNs, as was observed in an earlier study conducting whole-cell patch clamp recording of MNs in acute spinal cord slices taken from the same ALS and wild-type strains at 4 mo of age (8). Indeed, retrograde labeling of MNs by injection of TA and GC muscle (of wild-type mice) indicated these motor pools to be composed of predominantly fast-firing MNs, exactly the neurons lost as measured by slice recording by 4.5 mo. The inability of remaining MNs to precisely increase their firing frequency throughout a burst could be due to the fact that physiologically normal slow-type MNs do not have this capacity or that the synaptic drive and/or intrinsic properties of remaining MNs are altered. Nevertheless, it seems plausible that slower frequency firing of units that lack precisely timed increases in firing frequency could produce EMG output that is both less temporally precise (e.g., leading to cocontraction) and fractionated (i.e., lacks an underlying level of synchrony and/or sustained output from the upstream motor pool), with this EMG output manifesting as variability in muscle activity.

More specifically,

*i*) The loss of the fastest-firing MN population and many of the second-fastest-firing MNs by 4.5 mo of age, as discussed above, could potentially explain the entirety of the observed abnormal MN firing output in vivo. That is, this abnormal output is the appearance of a system seeking to activate fast-twitch muscles using mainly slow-firing MNs.

*ii*) Altered intrinsic properties of the remaining MNs in ALS mutants at 4.5 mo could also affect output. In the earlier slice study, there was a modest hyperpolarization of the fastest two of the remaining three MN populations at 4.5 mo, measuring ~6 mV (8). Perhaps in the context of unchanged resistance, this intrinsic alteration could increase the amount of synaptic current required to bring these cells to spiking threshold, potentially further decreasing attainable spike frequencies in the context of constant synaptic drive.

*iii*) Additionally, the overall circuit itself might be affected, for example, producing inadequate synaptic drive of the remaining MNs, preventing the cells from achieving high frequencies. Degeneration of the corticospinal tract, which contributes polysynaptic inputs, has been reported for G93A mice (figure 6 in ref. 12).

**Lack of MN Recruitment but Apparent Compensation.** The maintenance of stride length indicates that, despite the reduced firing of single MNs and fractionated EMGs, there must be either reserve or compensation to enable effective walking. To address whether recruitment of additional MNs within the lateral flexor/extensor motor pool might be a means of compensation, we conducted a c-Fos staining study (Fig. S10), which failed to observe a significant increase in the percentage of recruited firing neurons during walking on the wheel. Of course, it is unclear exactly what level of firing is required to induce c-Fos, so the study may underestimate

the collective of neurons and firing activity. However, it suggests that a strongly firing set of neurons remains a constant fraction of the pool and that, in the mutant, with the pool reduced by ∼50% due to MN loss, the number of strongly firing neurons is similarly reduced.

Thus, how do the mice compensate for this situation to maintain stride length? At the level of muscle, this could involve one or more the following observed features:

*i*) The increased cocontraction of lower leg muscles observed in the ALS mutant, involving simultaneous contraction of both TA and GC muscles (Fig. 4*B*), likely comprises a compensation, as observed in spinal injury patients (10).

*ii*) The earlier firing of the GC in ALS mutant mice (Fig. S6) compared with wild type may comprise a circuit adjustment that maintains posture and supports gait.

*iii*) The strong initial activity of both TA and GC muscle groups at step initiation likely also serves to maintain function (13).

At the level of spinal cord MNs, it remains likely that there must be some amount of compensated MN firing to maintain EMGs, the amplitude of which is similar to wild type, albeit irregular. We did not clearly observe such a feature in the extracellular recordings [see also in vivo study of Delestrée et al. (14)], but note that our study and that of Delestrée et al. (14) involved measurement from single neurons. There is an implication that, at the level of the entire motor pool, given that EMG is a measure of time of motor unit discharge, there must be more frequent firing. This would be reflected by earlier onset of GC activity and extended TA activity, for example. Multiunit recording might ultimately reveal such behavior.

## Materials and Methods

**Animals.** All animal handling and experimental procedures were approved by the Yale University Institutional Animal Care and Use Committee in accordance with National Institutes of Health guidelines for ethical treatment of animals. The G85R SOD1YFP (called 737) and wtSOD1YFP mouse strains have been previously described (15). The transgene is the entire human SOD1 gene, including the promoter, fused after the C-terminal codon to the YFP-coding sequence. The transgene copy number of all mutant animals was determined by RT-PCR using primer sets for human genomic SOD1 and mouse genomic ApoB, as recommended by Jackson Laboratories. Animals of the 737 strain that were used had measured copy numbers between 230 and 300.

**Daily Stride Length Measurements During Symptomatic Phase.** Mice were head-posted as described in *SI Materials and Methods*. After an initial acclimatization period on the wheel, mice were videotaped while walking spontaneously or being encouraged to walk by lightly brushing the tail. Videotaping was performed every other day from 4.5 mo of age until paralysis in G85R SOD1YFP ALS mice and in wtSOD1YFP mice until 6.5 mo of age. Videos for each day of tracking were viewed in MaxTraQ software. For each day, three steps were selected, and the MP joint was marked at the end of swing phase and at the end of stance phase. The *x*–*y* positions of both of these points were used to calculate the stride length of each step, and the average stride length for the session calculated.

**Kinematics/EMG.** Simultaneous kinematic and EMG recordings were carried out in head-posted mice (wired with EMG leads but lacking a spinal brace) walking on the wheel. Kinematics was monitored using IR-reflective microdots glued to joints of the left lower extremity with Vetbond: MP joint, ankle joint, knee joint, hip joint, and iliac crest. Videos were recorded with a high-speed VGA monochrome CMOS camera with USB 3.0 interface (XIMEA Corp., catalog no. MQ003MG-CM) at 350–450 frames per second. For these studies, reward-based training was not used, but mice were first acclimated by placement on the wheel for ∼1 h on each of 5 consecutive days before surgical installation of the EMG leads (*SI Materials and Methods*) and subsequent periods of recording. For monitoring EMG, the head-mounted pedestal was plugged into an amplifier (AM Systems Microelectrode Amplifier Model 1800). The signal was low-pass-filtered at 20 kHz, high-pass-filtered at 10 Hz, digitized at 50 kHz, and recorded via a Digidata 1440 interface (Molecular Devices). The data (Fig. 4) were processed as described in *SI Materials and Methods*.

**Single-Unit Recording from Spinal Cord.** For recording, borosilicate glass electrodes (World Precision Instruments) were pulled on a Brown Flaming puller (model P-97; Sutter Instruments). Pipettes filled with 0.9% sterile saline with 4–7 MΩ tip resistance were used. The pipette was positioned directly over the hole drilled in the glass window (see Fig. 1*B* for positioning) and brought to the surface of the spinal cord where the Z position of the micromanipulator was noted. The recording chamber, formed from a weigh boat and glued to the brace around the window, was filled with 0.9% sterile saline. Nine hundred to one thousand millibars of pressure was applied to the pipette to facilitate entry into the spinal tissue without clogging. The pipette was slowly brought to a depth of 500–700 μm with the micromanipulator before pressure was reduced to 50 millibars and resistance was checked to ensure an open tip. By slowly traveling the pipette through the column of tissue at this depth, single firing units were detected.

Recordings of single units were made in current clamp mode, and the electrical signal for unit recordings was low-pass-filtered at 10 kHz, high-pass-filtered at 200 Hz, digitized at 50 kHz, and recorded via a Digidata 1440 interface (Molecular Devices). Once a single firing unit was identified, the behavioral reinforcement loop was started to encourage walking (*SI Materials and Methods*), and recording was continued. Only one firing unit was recorded from each mouse. Data were processed as described in *SI Materials and Methods*.

**ACKNOWLEDGMENTS.** We thank Anthony DeSimone for excellent mechanical engineering support; Edward Zagha and David Salkoff for valuable discussion; James Howe and Wayne Fenton for critical reading of the manuscript; and Howard Hughes Medical Institute for generously supporting this work. M.H. was supported in part by the Nelson Fund; D.A.M. is supported by National Institute of Neurological Disorders and Stroke.

1. Robberecht W, Philips T (2013) The changing scene of amyotrophic lateral sclerosis. *Nat Rev Neurosci* 14(4):248–264.
2. Sreedharan J, Brown RH, Jr (2013) Amyotrophic lateral sclerosis: Problems and prospects. *Ann Neurol* 74(3):309–316.
3. Harms MB, Baloh RH (2013) Clinical neurogenetics: Amyotrophic lateral sclerosis. *Neurol Clin* 31(4):929–950.
4. Gurney ME, et al. (1994) Motor neuron degeneration in mice that express a human Cu,Zn superoxide dismutase mutation. *Science* 264(5166):1772–1775.
5. Bruijn LI, Miller TM, Cleveland DW (2004) Unraveling the mechanisms involved in motor neuron degeneration in ALS. *Annu Rev Neurosci* 27:723–749.
6. Pun S, Santos AF, Saxena S, Xu L, Caroni P (2006) Selective vulnerability and pruning of phasic motoneuron axons in motoneuron disease alleviated by CNTF. *Nat Neurosci* 9(3):408–419.
7. Hegedus J, Putman CT, Gordon T (2007) Time course of preferential motor unit loss in the SOD1 G93A mouse model of amyotrophic lateral sclerosis. *Neurobiol Dis* 28(2):154–164.
8. Hadzipasic M, et al. (2014) Selective degeneration of a physiological subtype of spinal motor neuron in mice with SOD1-linked ALS. *Proc Natl Acad Sci USA* 111(47):16883–16888.
9. Farrar MJ, et al. (2012) Chronic in vivo imaging in the mouse spinal cord using an implanted chamber. *Nat Methods* 9(3):297–302.
10. Gorassini MA, Norton JA, Nevett-Duchcherer J, Roy FD, Yang JF (2009) Changes in locomotor muscle activity after treadmill training in subjects with incomplete spinal cord injury. *J Neurophysiol* 101(2):969–979.
11. Hoffer JA, et al. (1987) Cat hindlimb motoneurons during locomotion. II. Normal activity patterns. *J Neurophysiol* 57(2):530–553.
12. Özdinler PH, et al. (2011) Corticospinal motor neurons and related subcerebral projection neurons undergo early and specific neurodegeneration in hSOD1G$^{93}$A transgenic ALS mice. *J Neurosci* 31(11):4166–4177.
13. Gorassini M, Bennett DJ, Kiehn O, Eken T, Hultborn H (1999) Activation patterns of hindlimb motor units in the awake rat and their relation to motoneuron intrinsic properties. *J Neurophysiol* 82(2):709–717.
14. Delestrée N, et al. (2014) Adult spinal motoneurones are not hyperexcitable in a mouse model of inherited amyotrophic lateral sclerosis. *J Physiol* 592(7):1687–1703.
15. Wang J, et al. (2009) Progressive aggregation despite chaperone associations of a mutant SOD1-YFP in transgenic mice that develop ALS. *Proc Natl Acad Sci USA* 106(5):1392–1397.
16. Christianson JA, Gebhart GF (2007) Assessment of colon sensitivity by luminal distension in mice. *Nat Protoc* 2(10):2624–2631.
17. McGinley MJ, David SV, McCormick DA (2015) Cortical membrane potential signature of optimal states for sensory signal detection. *Neuron* 87(1):179–192.
18. Bonilla E, et al. (1988) Duchenne muscular dystrophy: Deficiency of dystrophin at the muscle cell surface. *Cell* 54(4):447–452.
19. Akay T (2014) Long-term measurement of muscle denervation and locomotor behavior in individual wild-type and ALS model mice. *J Neurophysiol* 111(3):694–703.